arXiv:1408.4407v1 [nucl-th] 19 Aug 2014

Stellar $\beta^{\pm}$ decay rates of iron isotopes and its implications in astrophysics

Jameel-Un Nabi [1]

Faculty of Engineering Sciences, GIK Institute of Engineering Sciences and Technology, Topi 23640, NWFP, Pakistan

Abstract

β-decay and positron decay are believed to play a consequential role during the late phases of stellar evolution of a massive star culminating in a supernova explosion. The β-decay contributes in maintaining a respectable lepton-to-baryon ratio, Y_e, of the core prior to collapse which results in a larger shock energy to produce the explosion. The positron decay acts in the opposite direction and tends to decrease the ratio. The structure of the presupernova star is altered both by the changes in Y_e and the entropy of the core material. Recently the microscopic calculation of weak-interaction mediated rates on key isotopes of iron was introduced using the proton-neutron quasiparticle random phase approximation (pn-QRPA) theory with improved model parameters. Here I discuss in detail the improved calculation of $\beta^{\pm}$ decay rates for iron isotopes (^{54,55,56}Fe) in stellar environment. The pn-QRPA theory allows a microscopic "state-by-state" calculation of stellar rates as explained later in text. Excited state Gamow-Teller distributions are much different from ground state and a microscopic calculation of decay rates from these excited states greatly increases the reliability of the total decay rate calculation specially during the late stages of stellar evolution. The reported decay rates are also compared with earlier calculations. The positron decay rates are in reasonable agreement with the large-scale shell model calculation. The main finding of this work includes that the stellar β-decay rates of ^{54,55,56}Fe are around $3-5$ orders of magnitude smaller than previously assumed and hence irrelevant for the determination of the evolution of Y_e during the presupernova phase of massive stars. The current work discourages the inclusion of ^{55,56}Fe in the list of key stellar β-decay nuclei as suggested by former simulation results.

Key words: beta decay, GT strength distributions, pn-QRPA, core-collapse supernovas, massive stars
PACS: 21.60.Jz, 23.40.-s, 26.50.+x, 97.10.Cv

1 Introduction

The classical and pioneering works in the field of stellar physics include dynamics of supernova explosion by Baade & Zwicky (1), energy production in stars and stellar evolution by Bethe (2), and, synthesis of elements in stars by Burbidge et al. (3). Since then the microphysics of supernova explosion has come a long way. Whereas the strong interactions (fusion reactions) are responsible for providing the fuel to the stars empowering them throughout their life cycles, it is precisely the weak interactions that play a decisive role in determining both the presupernova stellar structure and the nucleosynthesis. The weak interaction reactions lead to the initiation of the gravitational collapse of the core of a massive star triggering a supernova explosion, control the lepton-to-baryon fraction of the core throughout the course of stellar evolution, play a key role in neutronisation of the core material, and, affect the formation of heavy elements above iron via the r-process at the final stage of the supernova explosion. Much to the advantage of the astrophysicists, the temperature during the late phases of stellar evolution is high enough for the matter composition to be given by nuclear statistical equilibrium. This means that one can get away with the need of reaction networks for the strong and electromagnetic interactions and the composition of the matter is given by the Saha equation.

Weak interactions in presupernova stars are known to be dominated by allowed Fermi (vector-type) and Gamow-Teller (axial-vector type) transitions. The calculation of weak-interaction rates is very sensitive to the distribution of the $GT_{\pm}$ strength function. In the GT_{+} strength a proton is changed into a neutron whereas the GT_{-} strength is responsible for transforming a neutron into a proton. It was Fuller, Fowler, and Newman (FFN) (4) who first performed an extensive calculation of stellar weak rates including the capture rates, decay rates, neutrino energy loss rates and gamma heating rates for a wide density and temperature domain. They performed their detailed calculation for 226 nuclei in the mass range $21 \leq A \leq 60$. The authors recognized the key role played by the GT giant resonance and noted that measured decay rates exploited only a small fraction of the total available strength. The centroids of the $GT_{\pm}$ distribution functions determine the effective energy of the capture and decay reactions. FFN estimated the GT contributions to the rates by a parametrization based on the independent particle model. Aufderheide et al. (5) later extended the FFN work for heavier nuclei with A $>$ 60

Email address: jameel@giki.edu.pk, jnabi@ictp.it
Telephone: 0092-938-271858
Fax: 0092-938-271890 (Jameel-Un Nabi).
[1] Current Address: The Abdus Salam ICTP, Strada Costiera 11, 34014, Trieste, Italy

and took into consideration the quenching of the GT strength neglected by FFN. Authors in Ref. (5) also stressed on the importance of β-decay rates in the iron core prior to the collapse. They tabulated the 71 top β-decay nuclei averaged throughout the stellar trajectory for $0.40 \leq Y_e \leq 0.5$ (see Table 26 of Ref. (5)). The measured data from various (p, n) and (n, p) experiments later revealed the misplacement of the GT centroids adopted in the parameterizations of FFN and subsequently used in the calculation of weak rates by Ref. (5). Since then theoretical efforts were concentrated on the microscopic calculations of weak-interaction mediated rates of iron-regime nuclide. Two such widely used models are the large-scale shell model (LSSM)(e.g. (6)) and the proton-neutron quasiparticle random phase approximation (pn-QRPA) theory (e.g. (7)).

The pn-QRPA theory is an efficient way to generate GT strength distributions which constitute a primary and nontrivial contribution to the weak-interaction mediated rates among iron-regime nuclide. The shell model calculations perform a detailed study of the nuclear spectroscopy, however, the pn-QRPA model has two important advantages. It can handle any arbitrarily heavy system of nucleons since the calculation is performed in a luxurious model space of up to 7 major oscillator shells. The second advantage is even more important for the calculation of weak-interaction rates in stellar matter. Because of the high temperatures prevailing during the presupernova and supernova phases of a massive star, there is a reasonable probability of occupation of parent excited states and the total weak interaction rates have a finite contribution form these excited states. Thus, in calculating a stellar rate, one must know the GT strength distributions of the excited states of the parent nucleus. As experimental information about excited state strength functions seems inaccessible, Aufderheide (8) stressed much earlier the need to probe these strength functions theoretically. The pn-QRPA model calculates the GT strength distribution strengths of *all* excited states of parent nucleus in a microscopic fashion and this feature of the pn-QRPA model greatly enhances the reliability of the calculated rates in stellar matter. These excited states are like resonances having finite band width and contributions from many discrete states calculated microscopically within the pn-QRPA framework. The construction of these excited states and calculation of the relevant nuclear matrix elements will be shown in the next section. In this sense the pn-QRPA model allows a fully microscopic "state-by-state" calculation of stellar weak rates. The calculation of stellar weak rates on iron-regime nuclei are sensitive to both the weak low-energy and strong high-energy ground and parent excited state GT strength distributions. The low energy part is more important during the earlier phase and the high energy part becomes important during the late phases of stellar evolution (8). Previous pn-QRPA calculations have shown that for certain nuclei the excited state rates can command the total weak rate (e.g. (9)). This clearly endorses the contribution of excited states in the calculation of total weak rates. Other calculations revert to approxima-

tions like the so-called Brink's hypothesis (in the electron capture direction) and back-resonances (in the β-decay direction). Brink's hypothesis states that GT strength distribution on excited states is *identical* to that from ground state, shifted *only* by the excitation energy of the state. GT back resonances are the states reached by the strong GT transitions in the inverse process (electron capture) built on ground and excited states.

Nabi and Klapdor-Kleingrothaus (10) first reported the calculation of weak interaction rates for 709 nuclei with A = 18 to 100 in stellar environment using the pn-QRPA theory. These included capture rates, decay rates, gamma heating rates, neutrino energy loss rates, probabilities of beta-delayed particle emissions and energy rate of these particle emissions. The authors then presented a detailed calculation of stellar weak interaction rates over a wide range of temperature and density scale for sd- (11) and fp/fpg-shell nuclei (7). These also included the weak interaction rates for nuclei with A = 40 to 44 (not yet calculated by shell model). Since then these calculations were further refined with use of more efficient algorithms, computing power, incorporation of latest data from mass compilations and experimental values, and fine-tuning of model parameters both in the sd- shell (12; 13; 14) and fp-shell (15; 9; 16; 17; 18; 19; 20) region. All theoretical calculations of stellar weak interactions have inherent uncertainties. The uncertainties associated with the pn-QRPA model were discussed in detail in Ref. (19). The reliability of the pn-QRPA calculation was discussed in length by Nabi and Klapdor-Kleingrothaus (7). There the authors compared the measured data (half lives and $B(GT_{\pm})$ strength) of thousands of nuclide with the pn-QRPA calculation and got fairly good comparison. Earlier half-lives of β^- decays were calculated systematically for about 6000 neutron-rich nuclei between the beta stability line and the neutron drip line using the pn-QRPA model (21). Similarly half-lives for β^+/EC (electron capture) decays for neutron-deficient nuclei with atomic numbers Z = 10 - 108 were calculated up to the proton drip line for more than 2000 nuclei using the same model (22). These microscopic calculations gave a remarkably good agreement with the then existing experimental data (within a factor of two for more than 90% (73%) of nuclei with experimental half-lives shorter than 1 s for β^- (β^+/EC) decays). Most nuclei of interest of astrophysical importance are the ones far from stability and one has to rely on theoretical models to estimate their beta decay properties. The accuracy of the pn-QRPA model increases with increasing distance from the β-stability line (shorter half-lives) (21; 22). This is a promising feature with respect to the prediction of experimentally unknown half-lives (specially those present in the stellar interior), implying that the predictions are made on the basis of a realistic physical model.

The isotopes of iron, ^{54,55,56}Fe, are mainly responsible for decreasing the electron-to-baryon ratio during the oxygen and silicon burning phases of massive stars through electron capture and positron decay processes. The electron

captures on these iron isotopes are the dominant process. Nevertheless, the β-decay rates for these isotopes of iron are also argued to be relevant during the presupernova evolution of massive stars in literature. Because of their astrophysical importance ^{55,56}Fe were included in the list of key β-decay nuclei that have a significant impact on the presupernova evolution of massive stars after core silicon burning for $0.47 \leq Y_e \leq 0.49$ compiled by Aufderheide and collaborators (see Tables 19, 20 and 26 of Ref. (5)). Later Heger and collaborators (23) studied the presupernova evolution of massive stars (of masses $15M_{\odot}, 25M_{\odot}$, and $40M_{\odot}$) and found ^{55}Fe in the list of top five nuclei that increase Y_e via β-decay and positron capture during the silicon burning phases of these massive stars. The authors employed the LSSM β-decay rates in their simulation code. The calculations of $\mathrm{GT}_{\pm}$ strength distributions and stellar weak rates for these isotopes of iron were introduced earlier using the pn-QRPA theory with improved model parameters (24). There the author was able to reproduce fairly well the experimental centroids and the total strength distributions in both directions for the even-even iron isotopes, ^{54,56}Fe where measurements were available. In this paper I discuss in detail the calculation of $\beta^{\pm}$ decay rates of ^{54,55,56}Fe in stellar environment and its astrophysical implications. The main finding of this work is that β-decay rates on ^{54,55,56}Fe are around 3 – 5 orders of magnitude smaller than previously assumed and are irrelevant for the determination of the evolution of Y_e during the presupernova phases of massive stars.

In the following section I briefly describe the theoretical formalism used to calculate the stellar electron and positron decay rates. The stellar $\beta^{\pm}$-decay rates of ^{54,55,56}Fe are presented in Section 3. Here I also compare the pn-QRPA decay rates with earlier calculations. Summary and conclusions are finally presented in Section 4.

2 Model Description

The calculation may be divided into three main steps. A Bogoliubov transformation was used to define quasiparticle states in terms of nucleon states and then the RPA equation was solved in the basis of proton-neutron quasiparticle pairs. The last step was to calculate the decay rates in stellar interior. The Hamiltonian for the calculation was of the form

$$H^{QRPA} = H^{sp} + V^{pair} + V^{ph}_{GT} + V^{pp}_{GT}. \tag{1}$$

The first step was approximated by a Nilsson + BCS calculation. Single-particle energies and wave functions were calculated in the Nilsson model, which takes into account nuclear deformation (25). Pairing was treated in

the BCS approximation. In the second step regarding the RPA calculation, both particle-hole (ph) and particle-particle (pp) GT forces were employed. The GT forces are appropriate for calculation of GT strength functions, since the transition amplitudes are closely connected to the forces. The particle-particle interaction, first considered by Cha (26), has usually been neglected in β^- decay (e.g. (21)) but is of decisive importance in β^+ decay (e.g. (27)). Both the particle-hole and particle-particle interaction can be given a separable form. The interactions were characterized by two interaction constants: χ (for particle-hole interaction) and κ (for particle-particle interaction). In this work, the values of χ and κ were taken as 0.15 MeV and 0.07 MeV, respectively. The value of the strength parameters was determined by a fit to the measured data (GT strengths and centroids) available for the isotopic chain. Other parameters required for the calculation of weak rates are the pairing gaps, the nuclear deformations and the Q-value of the nuclear reactions. I applied the traditional choice of $\Delta_p = \Delta_n = 12/\sqrt{A}(MeV)$ in this project (28). The deformation parameter was recently argued as an important parameter for QRPA calculations at par with the pairing parameter by Stetcu and Johnson (29). As such rather than using deformations from some theoretical mass model (as used in earlier calculations of pn-QRPA weak rates (11; 7)) the experimentally adopted values of the deformation parameters for ^{54,56}Fe, extracted by relating the measured energy of the first 2^+ excited state with the quadrupole deformation, were taken from Raman et al. (30). For the case of ^{55}Fe (where such measurement lacks) the deformation of the nucleus was calculated as

$$\delta = \frac{125(Q_2)}{1.44(Z)(A)^{2/3}}, \tag{2}$$

where Z and A are the atomic and mass numbers, respectively, and Q_2 is the electric quadrupole moment taken from Ref. (31). Q-values were taken from the recent mass compilation of Audi et al. (32).

The incorporation of measured deformations for ^{54,56}Fe and a smart choice of strength parameters led to an improvement of the calculated $GT_{\pm}$ distributions compared to the measured ones. Excited state calculation of $GT_{\pm}$ strengths was performed for a total of 246 parent states in ^{54}Fe, 297 states in ^{55}Fe and 266 states in ^{56}Fe, covering excitation energies in the vicinity of 15 MeV (as explained earlier). For each parent excited state, transitions were calculated to 150 daughter excited states. Daughter excitation energies up to around 20 MeV were considered in the calculation. The band widths of energy states were chosen according to the density of states of the concerned nucleus. In this way contribution from all excited states was incorporated in the calculation. A large model space assists in reproducing low-lying spectrum and higher excitations (33). The use of a separable interaction assisted in the incorporation of a luxurious model space of up to 7 major oscillator shells

which in turn made possible to consider these many excited states in both parent and daughter nuclei. In order to further increase the reliability of the calculated rates experimental data were incorporated in the calculation wherever possible. The calculated excitation energies were replaced with measured levels when they were within 0.5 MeV of each other. Missing measured states were inserted and inverse transitions (along with their logft values) were also taken into account. No theoretical levels were replaced with the experimental ones beyond the excitation energy for which experimental compilations had no definite spin and/or parity.

The beta decay (bd) and positron decay (pd) rates of a transition from the i^{th} state of the parent to the j^{th} state of the daughter nucleus are given by

$$\lambda_{ij}^{bd(pd)} = \left[\frac{\ln 2}{D}\right] \left[B(F)_{ij} + \left(g_A/g_V\right)_{eff}^2 B(GT)_{ij}\right] \left[f_{ij}^{bd(pd)}(T, \rho, E_f)\right]. \qquad (3)$$

The value of D was taken to be 6295s (34). B(F) and B(GT) are reduced transition probabilities of the Fermi and Gamow-Teller (GT) transitions, respectively,

$$B(F)_{ij} = \frac{1}{2J_i + 1} \mid< j \parallel \sum_k t_{\pm}^k \parallel i >\mid^2 . \qquad (4)$$

$$B(GT)_{ij} = \frac{1}{2J_i + 1} \mid< j \parallel \sum_k t_{\pm}^k \vec{\sigma}^k \parallel i >\mid^2 . \qquad (5)$$

Here $\vec{\sigma}^k$ is the spin operator and $t_{\pm}^k$ stands for the isospin raising and lowering operator. Details of the calculation of reduced transition probabilities can be found in Ref. (11). The effective ratio of axial and vector coupling constants, $(g_A/g_V)_{eff}$, which takes into account the observed quenching of the GT strength was taken to be (from Ref. (35)):

$$\left(\frac{g_A}{g_V}\right)_{eff}^2 = 0.60 \left(\frac{g_A}{g_V}\right)_{bare}^2 , \qquad (6)$$

with $(g_A/g_V)_{bare}$ = -1.254 (36). Interestingly, Vetterli and collaborators (37) and Rönnqvist et al. (38) predicted the same quenching factor of 0.6 for the RPA calculation in the case of ^{54}Fe when comparing their measured strengths to RPA calculation.

The $f_{ij}^{bd(pd)}$ are the phase space integrals and are functions of stellar temperature (T), density (ρ) and Fermi energy (E_f) of the electrons. They are

explicitly given by

$$f_{ij}^{bd} = \int_{1}^{w_m} w\sqrt{w^2-1}(w_m - w)^3 F(+Z,w)(1-G_-)dw, \tag{7}$$

and by

$$f_{ij}^{pd} = \int_{1}^{w_m} w\sqrt{w^2-1}(w_m - w)^3 F(-Z,w)(1-G_+)dw, \tag{8}$$

In Eqs. (7) and (8), w is the total energy of the electron including its rest mass. w_m is the total β-decay energy,

$$w_m = m_p - m_d + E_i - E_j, \tag{9}$$

where m_p and E_i are masses and excitation energies of the parent nucleus, and m_d and E_j of the daughter nucleus, respectively. F($\pm$ Z,w) are the Fermi functions and were calculated according to the procedure adopted by Gove and Martin (39). $G_\pm$ is the Fermi-Dirac distribution function for positrons (electrons).

$$G_+ = \left[\exp\left(\frac{E+2+E_f}{kT}\right)+1\right]^{-1}, \tag{10}$$

$$G_- = \left[\exp\left(\frac{E-E_f}{kT}\right)+1\right]^{-1}, \tag{11}$$

here E is the kinetic energy of the electrons and k is the Boltzmann constant.

The total decay rate per unit time per nucleus is finally given by

$$\lambda^{bd(pd)} = \sum_{ij} P_i \lambda_{ij}^{bd(pd)}, \tag{12}$$

where P_i is the probability of occupation of parent excited states and follows the normal Boltzmann distribution. After the calculation of all partial rates for the transition $i \rightarrow j$ the summation was carried out over all initial and final states until satisfactory convergence was achieved in the rate calculation.

Stellar decay rates are fragile functions of the available phase space, $(Q_\beta + E_i - E_j)$. Under terrestrial conditions, β-decay of ^{54,55,56}Fe is not possible (Q_β = -8.2430 MeV, -3.4520 MeV and -4.5660 MeV, for ^{54}Fe, ^{55}Fe and ^{56}Fe, respectively (32)). However, for stellar conditions the phase space can become

positive depending on the calculated energy eigenvalues of the underlying theoretical model. Construction of parent and daughter excited states and calculation of nuclear matrix elements in the pn-QRPA model is treated separately in the next section.

2.1 Calculation of excited states and nuclear matrix elements

The excited states in the pn-QRPA model can be constructed as phonon-correlated multi-quasi-particle states. The RPA is formulated for excitations from the $J^{\pi} = 0^{+}$ ground state of an even-even nucleus. The model extended to include the quasiparticle transition degrees of freedom yields decay half-lives of odd-mass and odd-odd parent nuclei with the same quality of agreement with experiment as for even-even nuclei (where only QRPA phonons contribute to the decays) (40). For the odd-A nucleus, ^{55}Fe, the ground state can be expressed as a one-quasiparticle state, in which the odd quasiparticle (q.p) occupies the single-q.p. orbit of the smallest energy. Then there exits two different type of transitions: phonon transitions with the odd neutron acting only as a spectator and transition of the odd neutron itself. For the later case, phonon correlations were introduced to one-quasiparticle states in first-order perturbation (41). The transition amplitudes between the multi-quasi-particle states can be reduced to those of single-quasi-particle states as shown below.

Excited states of even-even nucleus are obtained by one-proton (or one-neutron) excitations. They are described, in the quasiparticle (q.p.) picture, by adding two-proton (two-neutron) q.p.'s to the ground state (40). Excited states of ^{54,56}Fe are two-proton q.p. states and two-neutron q.p. states. Transitions from these initial states are possible to final proton-neutron q.p. pair states in the odd-odd daughter nucleus. The transition amplitudes and their reduction to correlated (c) one-q.p. states are given by

$$\begin{aligned} &< p^f n_c^f \mid t_{\pm}\sigma_{-\mu} \mid p_1^i p_{2c}^i > \\ &= -\delta(p^f, p_2^i) < n_c^f \mid t_{\pm}\sigma_{-\mu} \mid p_{1c}^i > + \delta(p^f, p_1^i) < n_c^f \mid t_{\pm}\sigma_{-\mu} \mid p_{2c}^i > \end{aligned} \tag{13}$$

$$\begin{aligned} &< p^f n_c^f \mid t_{\pm}\sigma_{\mu} \mid n_1^i n_{2c}^i > \\ &= +\delta(n^f, n_2^i) < p_c^f \mid t_{\pm}\sigma_{\mu} \mid n_{1c}^i > - \delta(n^f, n_1^i) < p_c^f \mid t_{\pm}\sigma_{\mu} \mid n_{2c}^i > \end{aligned} \tag{14}$$

where μ = -1, 0, 1, are the spherical components of the spin operator.

Four-proton (four-neutron) q.p. states and higher q.p. states were not considered in the model for the construction of excited states of ^{54,56}Fe. Higher q.p. states may affect the total decay rates specially at parent excitation energies

well in excess of 5 MeV. However the higher q.p. states were not considered in this calculation for consistency reasons. The model used for the calculation of weak-interaction rates was briefly introduced in Ref. (24). This model, along with the recipe to construct excited states as described in Ref. (40), was used to calculate electron and positron capture rates; electron and positron decay rates; and finally the neutrino and anti-neutrino cooling rates due to ^{54,55,56}Fe. It was reported in Ref. (24) that the calculated electron capture rates and neutrino cooling rates, using this model, was up to a factor four bigger than the corresponding LSSM rates (6) for the even-even isotopes of iron. Using the same model the calculated β-decay rates were found to be 3-5 orders of magnitude smaller (24) than the corresponding LSSM decay rates. The total decay rates are commanded mainly by the GT forces operating in the particle-particle and particle-hole channels. These forces were characterized by the interaction constants χ and κ as described previously. Work is currently in progress to include higher q.p. states in the construction of parent excited states to account for possible complicated configurations expected at high excitation energies. Any effect on the calculated β-decay rates due to inclusion of higher q.p. states would be reported in future.

When a nucleus has an odd nucleon (a proton and/or a neutron), some low-lying states are obtained by lifting the q.p. in the orbit of the smallest energy to higher-lying orbits (40). For ^{55}Fe nucleus, the excited states can be constructed
(1) by lifting the odd neutron from ground state to excited states (one-q.p. state),
(2) by three-neutron states, corresponding to excitation of a neutron (three-q.p. states), or,
(3) by one-neutron two-proton states, corresponding to excitation of a proton (three-q.p. states).

The formulae for multi-q.p. transitions and their reduction to correlated (c) one-q.p. states are given by,

$$\begin{aligned} &< p_1^f n_1^f n_{2c}^f \mid t_\pm \sigma_\mu \mid n_1^i n_2^i n_{3c}^i > \\ &= \delta(n_1^f, n_2^i)\delta(n_2^f, n_3^i) < p_{1c}^f \mid t_\pm \sigma_\mu \mid n_{1c}^i > -\delta(n_1^f, n_1^i)\delta(n_2^f, n_3^i) \\ &< p_{1c}^f \mid t_\pm \sigma_\mu \mid n_{2c}^i > +\delta(n_1^f, n_1^i)\delta(n_2^f, n_2^i) < p_{1c}^f \mid t_\pm \sigma_\mu \mid n_{3c}^i > \end{aligned} \tag{15}$$

$$\begin{aligned} &< p_1^f n_1^f n_{2c}^f \mid t_\pm \sigma_{-\mu} \mid p_1^i p_2^i n_{1c}^i > \\ &= \delta(p_1^f, p_2^i)[\delta(n_1^f, n_1^i) < n_{2c}^f \mid t_\pm \sigma_{-\mu} \mid p_{1c}^i > -\delta(n_2^f, n_1^i) \\ &< n_{1c}^f \mid t_\pm \sigma_{-\mu} \mid p_{1c}^i >] - \delta(p_1^f, p_1^i)[\delta(n_1^f, n_1^i) < n_{2c}^f \mid t_\pm \sigma_{-\mu} \mid p_{2c}^i > \\ &-\delta(n_2^f, n_1^i) < n_{1c}^f \mid t_\pm \sigma_{-\mu} \mid p_{2c}^i >] \end{aligned} \tag{16}$$

$$
\begin{aligned}
&< p_1^f p_2^f p_{3c}^f \mid t_\pm \sigma_\mu \mid p_1^i p_2^i n_{1c}^i > \\
&= \delta(p_2^f, p_1^i)\delta(p_3^f, p_2^i) < p_{1c}^f \mid t_\pm \sigma_\mu \mid n_{1c}^i > -\delta(p_1^f, p_1^i)\delta(p_3^f, p_2^i) \\
&< p_{2c}^f \mid t_\pm \sigma_\mu \mid n_{1c}^i > +\delta(p_1^f, p_1^i)\delta(p_2^f, p_2^i) < p_{3c}^f \mid t_\pm \sigma_\mu \mid n_{1c}^i > \qquad (17)
\end{aligned}
$$

Next I describe the construction of excited states of the daughter nuclei and the calculation of the respective matrix elements in the model. The low-lying states of an odd-proton even-neutron nucleus (daughter of ^{55}Fe) can be constructed,
(1) by exciting the odd proton from ground state (one-q.p. states),
(2) by three-proton states, corresponding to excitation of a proton (three-q.p. states), or,
(3) by one-proton two-neutron states, corresponding to excitation of a neutron (three-q.p. states).

The multi-q.p. transitions can again be reduced to correlated (c) one-q.p. states,

$$
\begin{aligned}
&< p_1^f p_2^f n_{1c}^f \mid t_\pm \sigma_{-\mu} \mid p_1^i p_2^i p_{3c}^i > \\
&= \delta(p_1^f, p_2^i)\delta(p_2^f, p_3^i) < n_{1c}^f \mid t_\pm \sigma_{-\mu} \mid p_{1c}^i > -\delta(p_1^f, p_1^i)\delta(p_2^f, p_3^i) \\
&< n_{1c}^f \mid t_\pm \sigma_{-\mu} \mid p_{2c}^i > +\delta(p_1^f, p_1^i)\delta(p_2^f, p_2^i) < n_{1c}^f \mid t_\pm \sigma_{-\mu} \mid p_{3c}^i > \qquad (18)
\end{aligned}
$$

$$
\begin{aligned}
&< p_1^f p_2^f n_{1c}^f \mid t_\pm \sigma_\mu \mid p_1^i n_1^i n_{2c}^i > \\
&= \delta(n_1^f, n_2^i)[\delta(p_1^f, p_1^i) < p_{2c}^f \mid t_\pm \sigma_\mu \mid n_{1c}^i > -\delta(p_2^f, p_1^i) \\
&< p_{1c}^f \mid t_\pm \sigma_\mu \mid n_{1c}^i >] - \delta(n_1^f, n_1^i)[\delta(p_1^f, p_1^i) < p_{2c}^f \mid t_\pm \sigma_\mu \mid n_{2c}^i > \\
&-\delta(p_2^f, p_1^i) < p_{1c}^f \mid t_\pm \sigma_\mu \mid n_{2c}^i >] \qquad (19)
\end{aligned}
$$

$$
\begin{aligned}
&< n_1^f n_2^f n_{3c}^f \mid t_\pm \sigma_{-\mu} \mid p_1^i n_1^i n_{2c}^i > \\
&= \delta(n_2^f, n_1^i)\delta(n_3^f, n_2^i) < n_{1c}^f \mid t_\pm \sigma_{-\mu} \mid p_{1c}^i > \ -\delta(n_1^f, n_1^i)\delta(n_3^f, n_2^i) \\
&< n_{2c}^f \mid t_\pm \sigma_{-\mu} \mid p_{1c}^i > \ +\delta(n_1^f, n_1^i)\delta(n_2^f, n_2^i) < n_{3c}^f \mid t_\pm \sigma_{-\mu} \mid p_{1c}^i > \qquad (20)
\end{aligned}
$$

For an odd-odd nucleus the ground state is assumed to be a proton-neutron q.p. pair state of smallest energy. Low-lying states in an odd-odd nucleus are expressed in the q.p. picture by proton-neutron pair states (two-q.p. states) or by states which are obtained by adding two-proton or two-neutron q.p.'s (four-q.p. states) (40). Therefore states in an odd-odd nucleus (daughter of ^{54,56}Fe) are expressed in q.p. transformation by two-q.p. states (proton-neutron pair states) or by four-q.p. states (two-proton or two-neutron q.p. states). Reduction of two-q.p. states into correlated (c) one-q.p. states is given as

$$
\begin{aligned}
&< p_1^f p_{2c}^f \mid t_\pm \sigma_\mu \mid p^i n_c^i > \\
&= \delta(p_1^f, p^i) < p_{2c}^f \mid t_\pm \sigma_\mu \mid n_c^i > - \delta(p_2^f, p^i) < p_{1c}^f \mid t_\pm \sigma_\mu \mid n_c^i > \qquad (21)
\end{aligned}
$$

$$
\begin{aligned}
&< n_1^f n_{2c}^f \mid t_\pm \sigma_{-\mu} \mid p^i n_c^i > \\
&= \delta(n_2^f, n^i) < n_{1c}^f \mid t_\pm \sigma_{-\mu} \mid p_c^i > - \delta(n_1^f, n^i) < n_{2c}^f \mid t_\pm \sigma_{-\mu} \mid p_c^i > \qquad (22)
\end{aligned}
$$

while the four-q.p. states are simplified as

$$
\begin{aligned}
&< p_1^f p_2^f n_1^f n_{2c}^f \mid t_\pm \sigma_{-\mu} \mid p_1^i p_2^i p_3^i n_{1c}^i > \\
&= \delta(n_2^f, n_1^i)[\delta(p_1^f, p_2^i)\delta(p_2^f, p_3^i) < n_{1c}^f \mid t_\pm \sigma_{-\mu} \mid p_{1c}^i > \\
&-\delta(p_1^f, p_1^i)\delta(p_2^f, p_3^i) < n_{1c}^f \mid t_\pm \sigma_{-\mu} \mid p_{2c}^i > + \delta(p_1^f, p_1^i)\delta(p_2^f, p_2^i) \\
&< n_{1c}^f \mid t_\pm \sigma_{-\mu} \mid p_{3c}^i >] - \delta(n_1^f, n_1^i)[\delta(p_1^f, p_2^i)\delta(p_2^f, p_3^i) < n_{2c}^f \mid t_\pm \sigma_{-\mu} \mid p_{1c}^i > \\
&-\delta(p_1^f, p_1^i)\delta(p_2^f, p_3^i) < n_{2c}^f \mid t_\pm \sigma_{-\mu} \mid p_{2c}^i > + \delta(p_1^f, p_1^i)\delta(p_2^f, p_2^i) \\
&< n_{2c}^f \mid t_\pm \sigma_{-\mu} \mid p_{3c}^i > \qquad (23)
\end{aligned}
$$

$$
\begin{aligned}
&< p_1^f p_2^f p_3^f p_{4c}^f \mid t_\pm \sigma_\mu \mid p_1^i p_2^i p_3^i n_{1c}^i > \\
&= -\delta(p_2^f, p_1^i)\delta(p_3^f, p_2^i)\delta(p_4^f, p_3^i) < p_{1c}^f \mid t_\pm \sigma_\mu \mid n_{1c}^i > \\
&+\delta(p_1^f, p_1^i)\delta(p_3^f, p_2^i)\delta(p_4^f, p_3^i) < p_{2c}^f \mid t_\pm \sigma_\mu \mid n_{1c}^i > \\
&-\delta(p_1^f, p_1^i)\delta(p_2^f, p_2^i)\delta(p_4^f, p_3^i) < p_{3c}^f \mid t_\pm \sigma_\mu \mid n_{1c}^i > \\
&+\delta(p_1^f, p_1^i)\delta(p_2^f, p_2^i)\delta(p_3^f, p_3^i) < p_{4c}^f \mid t_\pm \sigma_\mu \mid n_{1c}^i > \qquad (24)
\end{aligned}
$$

$$
\begin{aligned}
&< p_1^f p_2^f n_1^f n_{2c}^f \mid t_\pm \sigma_\mu \mid p_1^i n_1^i n_2^i n_{3c}^i > \\
&= \delta(p_1^f, p_1^i)[\delta(n_1^f, n_2^i)\delta(n_2^f, n_3^i) < p_{2c}^f \mid t_\pm \sigma_\mu \mid n_{1c}^i > \\
&-\delta(n_1^f, n_1^i)\delta(n_2^f, n_3^i) < p_{2c}^f \mid t_\pm \sigma_\mu \mid n_{2c}^i > + \delta(n_1^f, n_1^i)\delta(n_2^f, n_2^i) \\
&< p_{2c}^f \mid t_\pm \sigma_\mu \mid n_{3c}^i >] - \delta(p_2^f, p_1^i)[\delta(n_1^f, n_2^i)\delta(n_2^f, n_3^i) < p_{1c}^f \mid t_\pm \sigma_\mu \mid n_{1c}^i > \\
&-\delta(n_1^f, n_1^i)\delta(n_2^f, n_3^i) < p_{1c}^f \mid t_\pm \sigma_\mu \mid n_{2c}^i > + \delta(n_1^f, n_1^i)\delta(n_2^f, n_2^i) \\
&< p_{1c}^f \mid t_\pm \sigma_\mu \mid n_{3c}^i >] \qquad (25)
\end{aligned}
$$

$$
\begin{aligned}
&< n_1^f n_2^f n_3^f n_{4c}^f \mid t_\pm \sigma_{-\mu} \mid p_1^i n_1^i n_2^i n_{3c}^i > \\
&= +\delta(n_2^f, n_1^i)\delta(n_3^f, n_2^i)\delta(n_4^f, n_3^i) < n_{1c}^f \mid t_\pm \sigma_{-\mu} \mid p_{1c}^i > \\
&-\delta(n_1^f, n_1^i)\delta(n_3^f, n_2^i)\delta(n_4^f, n_3^i) < n_{2c}^f \mid t_\pm \sigma_{-\mu} \mid p_{1c}^i > \\
&+\delta(n_1^f, n_1^i)\delta(n_2^f, n_2^i)\delta(n_4^f, n_3^i) < n_{3c}^f \mid t_\pm \sigma_{-\mu} \mid p_{1c}^i > \\
&-\delta(n_1^f, n_1^i)\delta(n_2^f, n_2^i)\delta(n_3^f, n_3^i) < n_{4c}^f \mid t_\pm \sigma_{-\mu} \mid p_{1c}^i > \qquad (26)
\end{aligned}
$$

For all the given q.p. transition amplitudes [Eqs. (13)- (26)], the antisymmetrization of the single- q.p. states was taken into account:
$p_1^f < p_2^f < p_3^f < p_4^f$,
$n_1^f < n_2^f < n_3^f < n_4^f$,
$p_1^i < p_2^i < p_3^i < p_4^i$,
$n_1^i < n_2^i < n_3^i < n_4^i$.
GT transitions of phonon excitations for every excited state were also taken into account. Here I assumed that the quasiparticles in the parent nucleus remained in the same quasiparticle orbits. A detailed description of the formalism can be found in Ref. (40).

3 Results and discussion

The improved pn-QRPA model, as described in the previous section, was used to calculate the $GT_{\pm}$ strength distributions of iron isotopes in astrophysical conditions. The model incorporated experimental excitation energies, $\log ft$ values and deformations as discussed earlier. The GT strength distributions (in both directions) were calculated for ground and 245 excited states in ^{54}Fe, 296 excited states in ^{55}Fe and 265 excited states in ^{56}Fe. The model was tested for the case of ^{54,56}Fe where measured distributions were available. It was shown in Ref. (24) that the comparison of $GT_{\pm}$ strength distributions for ^{54,56}Fe with measured data was very good (e.g. the total $B(GT_{-})$ strength for ^{54}Fe calculated within the framework of Ref. (7) was 9.33 which was narrowed down to 7.56 using the improved model of pn-QRPA (24) in comparison with the measured value of 7.5 $\pm$ 0.7 (42)). The $GT_{\pm}$ strength distributions for ground and all excited states of iron isotopes are available as ASCII files and can be requested from the author.

In order to highlight the important role of parent excited states in the calculation of total decay rates, I present in Table 1 the values of the total beta decay (λ_{bd}) and positron decay (λ_{pd}) rates with contributions from all excited states in units of s^{-1}. These rates are calculated at selected values of astrophysical temperature and density shown in first column (the first number within the parenthesis gives the value of density in units of gcm^{-3} and the second number denotes the stellar temperature in units of 10^9 K). It is to be noted that the corresponding ground-state beta and positron decay rates are energetically forbidden. The excited states play a key role in the calculation of total decay rates which are very sensitive to the available phase space ($= Q_{\beta} + E_i - E_j$). The construction of excited states in the pn-QRPA model was discussed in the previous section. The phase space integrals given in Eq. (3) increase considerably at higher stellar temperatures and cause orders of magnitude enhancement in the calculated decay rates. Fine grid calculation of positron and β-decay rates for iron isotopes as a function of stellar tem-

perature, density and Fermi energy, suitable for core-collapse simulations and interpolation purposes, is available as ASCII files and can be requested from the author.

Figures 1, 2 and 3 show the calculated β-decay rates for ^{54,55,56}Fe, respectively. Each figure shows four panels depicting the calculated β-decay rates at selected temperature and density domain. The upper left panel shows the decay rates in low-density region ($\rho Y_e[gcm^{-3}] = 10^{0.5}, 10^{1.5}$ and $10^{2.5}$), the upper right in medium-low density region ($\rho Y_e[gcm^{-3}] = 10^{3.5}, 10^{4.5}$ and $10^{5.5}$), the lower left in medium-high density region ($\rho Y_e[gcm^{-3}] = 10^{6.5}, 10^{7.5}$ and $10^{8.5}$) and finally the lower right panel depicts the calculated rates in high density region ($\rho Y_e[gcm^{-3}] = 10^{9.5}, 10^{10.5}$ and 10^{11}) of stellar core of massive stars. The decay rates are given in logarithmic scales (to base 10) in units of s^{-1}. T_9 gives the stellar temperature in units of 10^9 K. One should note the orders of magnitude increment in β-decay rates as the stellar temperature increases. The rates are almost superimposed on one another as a function of stellar density in the first three panels. This means that there is no appreciable change in the β-decay rates when increasing the density by an order of magnitude. However as the stellar matter moves from the medium high density region to high density region these rates start to 'peel off' from one another. In high density regions the rates start to decrease appreciably due to a decrease in the phase space. There is a sharp exponential increase in the decay rates as the stellar temperature increases up to $\sim T_9 = 5$. Beyond this temperature the slope of the rates reduces drastically with increasing density. For a given density the β-decay rates increase monotonically with increasing temperatures. The calculated stellar β-decay rates are smallest for ^{54}Fe and biggest for ^{55}Fe. The calculated β-decay rates are smaller in magnitude compared to the corresponding positron capture rates (in the same direction) on these iron isotopes.

Figures 4, 5 and 6 again show four panels depicting the calculated positron decay rates at selected temperature and density domain for ^{54,55,56}Fe, respectively. The upper left panel shows the positron decay rates in low-density region ($\rho Y_e[gcm^{-3}] = 10^{0.5}, 10^{1.5}$ and $10^{2.5}$), the upper right in medium-low density region ($\rho Y_e[gcm^{-3}] = 10^{3.5}, 10^{4.5}$ and $10^{5.5}$), the lower left in medium-high density region ($\rho Y_e[gcm^{-3}] = 10^{6.5}, 10^{7.5}$ and $10^{8.5}$) and finally the lower right panel depicts the calculated positron decay rates in high density region ($\rho Y_e[gcm^{-3}] = 10^{9.5}, 10^{10.5}$ and 10^{11}) of the stellar core. The rates are given in logarithmic scales (to base 10) in units of s^{-1}. The calculated positron decay rates are greater than the corresponding β-decay rates by orders of magnitude. Due to an increase in phase space with increasing temperature, the positron decay rates increase by orders of magnitude as T_9 increases. The increase is exponential up to $\sim T_9 = 5$. As temperature rises (the degeneracy parameter is negative for positrons), more and more high-energy positrons are created leading in turn to higher decay rates. It can be seen from these figures that

the positron decay rates are almost the same as functions of the core density. The positron decay rates are biggest for ^{55}Fe and smallest for ^{56}Fe. It is worth mentioning that the beta and positron decay rates are very small numbers and can change by orders of magnitude by a mere change of 0.5 MeV, or less, in parent or daughter excitation energies (as the rates are very sensitive to the available Q_β window) and are more reflective of the uncertainties in the calculation of energies.

It would be interesting to know how the reported decay rates of iron isotopes compare with earlier calculations for temperature and density domains of astrophysical interest. For the sake of comparison I took into consideration the pioneer calculations of FFN (4) and those performed using the large-scale shell model (LSSM) (6). The FFN rates were used in many simulation codes (e.g. KEPLER stellar evolution code (43)) while LSSM rates were employed in recent simulation of presupernova evolution of massive stars in the mass range 11-40 $M_\odot$ (23).

Positron decay rates of iron isotopes may decrease the Y_e value of massive stars. As mentioned before, the positron decay rate calculations do not differ appreciably by changing densities. Figure 7 depicts the comparison of positron decay rates for ^{54}Fe with earlier calculations. The upper panel displays the ratio of calculated rates to the LSSM rates, $R_{pd}(QRPA/LSSM)$, while the lower panel shows a similar comparison with the FFN calculation, $R_{pd}(QRPA/FFN)$. The comparison is made for the selected temperature and density domain. Here one sees that the pn-QRPA and LSSM calculations are in overall reasonable agreement. The comparison is good at low temperatures while at higher temperatures, $T_9 > 5$, the LSSM rates are bigger around an order of magnitude. The FFN rates are much bigger than the reported positron decay rates by $1 - 2$ orders of magnitude. It is reminded that FFN neglected the quenching of the GT strength in their rate calculation. Further FFN did not take into effect the process of particle emission from excited states and their parent excitation energies extended well beyond the particle decay channel. These high lying excited states began to show their cumulative effect at high temperatures and densities.

The comparison of reported positron decay rates of ^{55}Fe with LSSM calculation is somewhat different. For the first time one sees that the pn-QRPA calculated positron decay rate is bigger than LSSM (Figure 8). This however is true only for $T_9 = 1$. During the early phases of presupernova evolution the reported positron decay rates are bigger than LSSM rates by an order of magnitude. For successive stages, $1.5 \leq T_9 \leq 5$, the two calculations are in good agreement. At still higher temperatures the LSSM rates exceed by more than an order of magnitude. Excited state GT distributions in ^{55}Fe play a key role in determining the total decay rate at various stages of presupernova evolution. It is reminded that the pn-QRPA makes a microscopic assessment of

GT strength distribution for all such parent excited states. Comparison with the FFN rates is fairly constant. It is to be noted that the ratios are shown on a linear scale (bottom panel of Figure 8). At $T_9 = 10$, the FFN rates surpass the reported rates for reasons already mentioned.

The comparison of reported positron decay rates of ^{56}Fe with previous calculations is shown in Figure 9. The LSSM decay rates are bigger by as much as a factor of 20 (the comparison is better at low temperatures). The lower panel of Figure 9 shows a whopping enhancement in the calculated positron decay rates of ^{56}Fe of around 13 orders of magnitude compared to FFN rates at low temperatures. However there are reasons for this unusual suppression of FFN positron decay rates. Unmeasured matrix elements for allowed transitions were assigned an average value of $logft$ =5 in FFN calculations. Later, (n, p) experiments were performed for ^{56}Fe (38; 44) which revealed a too small $logft$ value assignment for allowed transitions employed by FFN. Consequently the FFN rates are much too smaller than the LSSM and pn-QRPA calculations at low temperatures (LSSM rates are also bigger than FFN rates by roughly 13 orders of magnitude at $T_9 = 1.5$). The LSSM positron decay rates for iron isotopes are bigger up to a factor of 20 as compared to the pn-QRPA rates. The overall comparison of positron decay rates of ^{54,55,56}Fe shows that the calculated rates are in reasonable agreement with the LSSM calculated rates. Major differences are seen in the case of the β-decay rate calculations and are discussed in detail below.

Authors in Ref. (6) reported that, for even-even and odd-A nuclei, FFN systematically placed the back resonance at much lower energies and concluded that contribution of the back resonances to the β-decay rates for these nuclei decreases. They estimated that LSSM β-decay rates as a result were smaller, on the average, by a factor of 20 (40) as compared to the FFN β-decay rates for even-even (odd-A) nuclei.

Figure 10 depicts the comparison of β-decay rates for ^{54}Fe with earlier calculations. As before the upper panel displays the ratio of calculated rates to the LSSM rates, $R_{bd}(QRPA/LSSM)$, while the lower panel shows a similar comparison with the FFN calculation, $R_{bd}(QRPA/FFN)$. The density scale is shown in the inset. A mutual comparison of LSSM and FFN β-decay rates for the case of ^{54}Fe reveals that for low temperatures ($T_9 < 2$) and densities $\rho Y_e[gcm^{-3}] \sim 10^6 - 10^7$ the LSSM β-decay rates are bigger than the FFN rates by as much as four orders of magnitude. Only at higher temperatures and densities are the LSSM rates smaller than the FFN rates (by around an order of magnitude). The LSSM β-decay rates for ^{54}Fe are 3 – 4 orders of magnitude bigger than the pn-QRPA rates for the physical conditions depicted in Figure 10. The enhancement ratio increases with increasing densities. The reasons for bigger LSSM β-decay rates are not very clear. The Q-values and phase space formulation for the two calculations appear the same. Perhaps

the contribution from back resonances needs a further cut back in the LSSM calculation for the β-decay of even-even and odd-A nuclei (i.e. the back resonances for these nuclei should be put at even higher energies than calculated by LSSM). As mentioned before the reported rates do not employ these approximations and calculate all the excited state GT strength distributions in a microscopic fashion. The comparison with the FFN rates reveals that the reported decay rates are smaller by as much as four orders of magnitude (at higher temperatures). At temperature $T_9 = 1$ and density $\rho Y_e[gcm^{-3}] = 10^6$, where the LSSM β-decay rates are bigger than the FFN rates by roughly four orders of magnitude, the reported rates are bigger than the FFN rates by an order of magnitude. For all other points the FFN rates are much bigger than pn-QRPA rates for reasons mentioned before.

The β-decay rates of ^{55}Fe are believed to be important during the silicon burning stages of massive stars as per the simulation results of Ref. (23). Figure 11 shows a comparison of the three calculations for β-decay rates of ^{55}Fe during the relevant temperature and density domain of stellar core. Only at low temperatures and densities are the LSSM decay rates smaller than the corresponding FFN numbers. At higher temperatures ($T_9 \geq 5$) and densities ($\rho Y_e[gcm^{-3}] > 10^7$) the LSSM rates surpass the FFN decay rates by more than two orders of magnitude. The comparison of pn-QRPA rates with LSSM suggests that the LSSM rates are bigger by 2 – 3 orders of magnitude (at lower densities the comparison is relatively better) . In fact the LSSM β-decay rates are even bigger than their calculated positron capture rates (only at higher temperatures their positron capture rates surpass the β-decay rates). In contrast the pn-QRPA calculated β-decay rates are suppressed as compared to the corresponding positron capture rates for all temperature and density scales. At higher densities the LSSM β-decay rates are bigger by 3 – 5 orders of magnitude. The FFN rates are up to four orders of magnitude bigger than the pn-QRPA rates for reasons mentioned before.

A study of LSSM and the FFN rates reveals that LSSM β-decay rates of ^{56}Fe are much bigger than the FFN rates at high temperatures and densities (by more than an order of magnitude). Figure 12 shows how the reported β-decay rates of ^{56}Fe compare with earlier calculations for relevant physical conditions. It can be seen from the figure that the reported rates are much smaller (up to four orders of magnitude) than previous calculations. Comparison with LSSM calculation shows that at higher densities the reported β-decay rates are suppressed by up to three orders of magnitude. At higher temperatures (T_9 = 30) the comparison ratio improves. However the LSSM rates are still bigger by around an order of magnitude. On the other hand the FFN rates are bigger than the reported β-decay rates by around four orders of magnitude at lower densities and temperatures. The comparison ratio improves with increasing temperatures and densities. The pn-QRPA rates are bigger than the FFN rates by around a factor of 8 at $T_9 = 30$. The comparison study of stellar β-

decay rates of iron isotopes suggests that the LSSM β-decay rates are bigger than the corresponding pn-QRPA rates by 3 – 5 orders of magnitude.

Earlier using the same model the electron capture rates due to ^{54,55,56}Fe were calculated and were found to be in overall good comparison with the LSSM electron capture rates (24). In fact the pn-QRPA electron capture rates on ^{54}Fe were around a factor three bigger than LSSM rates in the relevant astrophysical conditions (see Table 3 of Ref. (24)). Using the same model, however, the calculated β-decay rates are smaller by 3 – 5 orders of magnitude. This suppression in the pn-QRPA β-decay rates comes from the excited state GT distributions (smaller nuclear matrix elements) which are much different from the ground state distribution. In order to gain a detailed insight of these distributions I took a representative temperature and density point of $T_9 = 10$ and $\rho Y_e[gcm^{-3}] = 10^7$ (weak interaction rates due to iron isotopes are argued to contribute effectively around such physical conditions during the presupernova evolution of massive stars). Table 2 shows the data of the ground and first four excited states that have a finite partial decay rate contribution to the total β-decay rate of ^{54,55,56}Fe within the framework of the model of magnitude greater than $10^{-25}s^{-1}$. The first column shows the calculated parent excited energy state in units of MeV, the second column gives the product of occupation probability and partial β-decay rate from this state in units of s^{-1}. The third and fourth column give the centroid and total B(GT) strength, respectively, from this parent state. The cut-off energy in daughter nuclei is 12 MeV. It can be seen clearly from Table 2 that for the even-even isotopes the centroids of the excited state GT strength distributions are shifted to much higher energies in the daughter. The ΣS_{β^-} strengths are also considerably smaller from the corresponding ground state strengths. These are mainly responsible for the smaller total β-decay rates. The excited state GT strength distributions are also much different from the ground state distribution for the case of ^{55}Fe. The excited state GT distributions for ^{54,55,56}Fe are shown graphically in Figures 13, 14 and 15, respectively. The ground state GT strength distributions were presented earlier in Ref. (24). Here I have shown only the first three excited state distributions that have a finite partial decay rate contribution of magnitude greater than $10^{-25}s^{-1}$. Note the different scales of the B(GT) strength values in the vertical panels of these figures. From these figures it is clear that the Brink's hypothesis (and back resonances for the calculation of β-decay) is not a good approximation for calculation of stellar weak interaction rates of iron isotopes. These and similar finite partial decay rates lead to an overall suppression in the total β-decay rate which happens to be 5.44E-09 s^{-1}, 4.32E-07 s^{-1} and 2.62E-05 s^{-1} for ^{54}Fe, ^{55}Fe and ^{56}Fe, respectively, under the physical conditions stated above.

4 Summary and conclusions

Capture and decay rates are considered to be very important in controlling the lepton-to-baryon ratio and entropy of the core of massive stars during the presupernova evolutionary phases. These are the two key parameters which later play a key role in the dynamics of supernova explosion. A reliable and microscopic calculation of these weak interaction rates can assist us in a better understanding of the explosion process.

The pn-QRPA model has a very good rapport in calculation of beta decay rates. The model has access to a huge model space of seven major shells and is the only available model to perform a fully microscopic 'state-by-state' calculation of weak rates in stellar interior. The stellar electron and positron β-decay rates of iron isotopes were presented using the pn-QRPA model. Incorporation of latest experimental data and an optimum selection of model parameters increased the reliability of the calculated rates. The calculated rates were also compared with previous calculations.

The key findings of this work include that the Brink's hypothesis and back resonances used in previous calculations of decay rates for iron isotopes are not a good approximation to use. A microscopic calculation of excited state GT strength distributions greatly increases the reliability of calculated rates. The β-decay rates calculated by large scale shell model calculation are $3-5$ orders of magnitude bigger than the reported rates in astrophysical conditions. The microscopic calculation of excited state GT strength distribution calculated within the framework of the pn-QRPA model, which are responsible for the reduced β-decay rates, was also discussed. During the early phases of presupernova evolution the LSSM calculated β-decay rates are even bigger than the competing positron capture rates (both occur in the same direction and tend to decrease Y_e). The pn-QRPA calculated β-decay rates are smaller than the competing positron capture rates. FFN β-decay rates are up to four orders of magnitude bigger than the reported rates under the same conditions. The pn-QRPA calculation validates the finding by authors in Ref. (6) that FFN places the so-called back resonances at too low excitation energies in even-even and odd-A nuclei. The reported calculation also suggests that the placement of back resonances employed by LSSM needs further push towards higher excitation energies. The LSSM positron decay rates are, comparatively, in reasonable agreement with the pn-QRPA rates.

What may be the astrophysical implications of the reported decay rates of iron isotopes? The β-decay rates of iron nuclei are much smaller than previously assumed and this news is important for core-collapse simulators world-wide. The current study suggests that β-decay rates of iron isotopes are irrelevant for the determination of the evolution of Y_e during the presupernova

phase of massive stars. A review of inclusion of iron isotopes ^{55,56}Fe in the list of key stellar β-decay nuclei as suggested by previous simulation results (5; 23) is in order.

Acknowledgments: The author would like to acknowledge the kind hospitality provided by the Abdus Salam ICTP, Trieste, where part of this project was completed. The author also wishes to acknowledge the support of research grant provided by the Higher Education Commission Pakistan, through the HEC Project Nos. 20-1171 and 20-1283.

References

[1] Baade W. & Zwicky F., On Supernovae, *Proc. Nat. Acad. Sci.*, 20, 254-259, 1934.

[2] Bethe H. A., Energy Production in Stars, *Phys. Rev.*, 55, 434-456, 1939.

[3] Burbidge E. M., Burbidge G. R., Fowler W. A. & Hoyle F., Synthesis of the Elements in Stars, *Rev. Mod. Phys*, 29, 547-650, 1957.

[4] Fuller G. M., Fowler W. A. & Newman M. J., Stellar Weak-Interaction Rates for sd-Shell Nuclei. I. Nuclear Matrix Element Systematics with Application to ^{26}Al and Selected Nuclei of Importance to the Supernova Problem, *Astrophys. J. Suppl.*, 42, 447-473, 1980; Stellar Weak Interaction Rates for Intermediate Mass Nuclei. II. A = 21 to A = 60, *Astrophys. J.*, 252, 715-740, 1982; Stellar Weak Interaction Rates for Intermediate Mass Nuclei. III. Rate Tables for the Free Nucleons and Nuclei with A = 21 to A = 60, *Astrophys. J. Suppl.*, 48, 279-320, 1982; Stellar Weak Interaction Rates for Intermediate Mass Nuclei. IV. Interpolation Procedures for Rapidly Varying Lepton Capture Rates Using Effective log (ft)- Values, *Astrophys. J.*, 293, 1-16, 1985.

[5] Aufderheide M. B., Fushiki I., Woosley S. E., Stanford E. & Hartmann D. H., Search for Important Weak Interaction Nuclei in Presupernova Evolution, *Astrophys. J. Suppl. Ser*, 91, 389-417, 1994.

[6] Langanke K. & Martínez-Pinedo G., Shell-Model Calculations of Stellar Weak Interaction Rates: II. Weak Rates for Nuclei in the Mass Range A = 45-65 in Supernovae Environments, *Nucl. Phys.*, A673, 481-508, 2000.

[7] Nabi J.-Un & Klapdor-Kleingrothaus H. V., Microscopic Calculations of Stellar Weak Interaction Rates and Energy Losses for fp- and fpg-Shell Nuclei, *At. Data Nucl. Data Tables*, 88, 237-476, 2004.

[8] Aufderheide M. B., Stellar Electron Capture Rates and the ^{54}Fe(n,p) Experiment, *Nucl. Phys.*, A526, 161-187, 1991.

[9] Nabi J.-Un & Sajjad M., Comparative Study of Gamow-Teller Strength Distributions in the Odd-odd Nucleus ^{50}V and its Impact on Electron Cap-

ture Rates in Astrophysical Environments, *Phys. Rev. C*, 76, 055803-1 - 055803-8, 2007.

[10] Nabi J.-Un & Klapdor-Kleingrothaus H. V., Microscopic Calculations of Weak Interaction Rates of Nuclei in Stellar Environment for A = 18 to 100, *Eur. Phys. J. A*, 5, 337-339, 1999.

[11] Nabi J.-Un & Klapdor-Kleingrothaus H. V., Weak Interaction Rates of sd-Shell Nuclei in Stellar Environments Calculated in the Proton-Neutron Quasiparticle Random-Phase Approximation, *At. Data Nucl. Data Tables*, 71, 149-345, 1999.

[12] Nabi J.-Un & Rahman M.-Ur, Gamow-Teller Transitions from ^{24}Mg and Their Impact on the Electron Capture Rates in the O+Ne+Mg Cores of Stars, *Phys. Rev. C*, 75, 035803-1 - 035803-5, 2007.

[13] Nabi J.-Un, Stellar Neutrino Loss Rates due to ^{24}Mg Suitable for O+Ne+Mg Core Simulations, *Phys. Rev. C*, 78, 045801-1 045801-11, 2008.

[14] Nabi J.-Un, Detailed Microscopic Calculation of Stellar Electron and Positron Capture Rates on ^{24}Mg for O+Ne+Mg Core Simulations, *Phys. Scripta*, 78, 035201-1 - 035201-10, 2008.

[15] Nabi J.-Un & Rahman M.-Ur, Gamow-Teller Strength Distributions and Electron Capture Rates for ^{55}Co and ^{56}Ni, *Phys. Lett*, B612, 190-196, 2005.

[16] Nabi J.-Un, Sajjad M. & Rahman M.-Ur, Electron Capture Rates on Titanium Isotopes in Stellar Matter, *Acta Phys. Pol. B*, 38, 3203-3223, 2007.

[17] Nabi J.-Un, Rahman M.-Ur & Sajjad M., Electron and Positron Capture Rates on ^{55}Co in Stellar Matter, *Braz. J. Phys.*, 37, 1238-1245, 2007.

[18] Nabi J.-Un, Rahman M.-Ur & Sajjad M., Gamow-Teller ($GT_{\pm}$) Strength Distributions of ^{56}Ni for Ground and Excited States, *Acta Phys. Pol. B*, 39, 651-669, 2008.

[19] Nabi J.-Un & Sajjad M., Neutrino Energy Loss Rates and Positron Capture Rates on ^{55}Co for Presupernova and Supernova Physics, *Phys. Rev. C*, 77, 055802-1 - 055802-13, 2008.

[20] Nabi J.-Un & Sajjad M., Expanded Calculations of Proton-Neutron Quasiparticle Random Phase Approximation (pn-QRPA) Electron Capture Rates on ^{55}Co for Presupernova and Supernova Physics *Can. J. Phys*, 86, 819-828, 2008.

[21] Staudt A., Bender E., Muto K. & Klapdor-Kleingrothaus H. V., Second-Generation Microscopic Predictions of Beta-Decay Half-lives of Neutron-Rich Nuclei, *At. Data Nucl. Data Tables*, 44, 79-132, 1990.

[22] Hirsch M., Staudt A., Muto K. & Klapdor-Kleingrothaus H. V., Microscopic Predictions of β^+/EC-Decay Half-Lives, *At. Data Nucl. Data Tables*, 53, 165-193, 1993.

[23] Heger A., Woosley S. E., Martínez-Pinedo G. & Langanke K., Presupernova Evolution with Improved Rates for Weak Interactions, *Astrophys. J.*, 560, 307-325, 2001.

[24] Nabi J.-Un, Weak-Interaction-Mediated Rates on Iron Isotopes for Presupernova Evolution of Massive Stars, *Eur. Phys. J. A*, 40, 223-230, 2009.

[25] Nilsson S. G., Binding States of Individual Nucleons in Strongly Deformed Nuclei, *Mat. Fys. Medd. Dan. Vid. Selsk*, 29, 1-68, 1955.
[26] Cha D., $\sigma\tau_+$ Strength in Nuclei, *Phys. Rev. C*, 27, 2269-2281, 1983.
[27] Staudt A., Hirsch M., Muto K. & Klapdor-Kleingrothaus H. V., Calculation of β-Delayed Fission of ^{180}Tl and Application of the Quasiparticle Random-Phase Approximation to the Prediction of β^+-Decay Half-Lives of Neutron-Deficient Isotopes, *Phys. Rev. Lett.*, 65, 1543-1546, 1990.
[28] Hirsch M., Staudt A., Muto K. & Klapdor-Kleingrothaus H. V., Microscopic Calculation of β^+/EC-Decay Half-Lives with Atomic Numbers Z = 10-30, *Nucl. Phys.*, A535, 62-76, 1991.
[29] Stetcu I. & Johnson C. W., Gamow-Teller Transitions and Deformation in the Proton-Neutron Random Phase Approximation, *Phys. Rev. C*, 69, 024311-1 - 024311-7, 2004.
[30] Raman S., Malarkey C. H., Milner W. T., Nestor, Jr. C. W. & Stelson P. H., Transition Probability, B(E2)↑, from the Ground to the First-Excited 2^+ State of Even-Even Nuclides, *At. Data Nucl. Data Tables*, 36, 1-96, 1987.
[31] Möller P. & Nix J. R., Atomic Masses and Nuclear Ground-State Deformations Calculated with a New Macroscopic-Microscopic Model, *At. Data Nucl. Data Tables*, 26, 165-196, 1981.
[32] Audi G., Wapstra A. H. & Thibault C., The AME2003 Atomic Mass Evaluation (II). Tables, Graphs and References, *Nucl. Phys.*, A729, 337-676, 2003.
[33] Haxton W. C. & Johnson C., Weak-Interaction Rates in ^{16}O, *Phys. Rev. Lett.*, 65, 1325-1328, 1990.
[34] Yost G. P., Barnett R. M., Hinchliffe I., *et al.* (Particle Data Group), Review of Particle Properties, *Phys. Lett.*, B204, 1-476, 1988.
[35] Gaarde C., Gamow-Teller and M1 Resonances, *Nucl. Phys.*, A396, 127c-144c, 1983.
[36] Rodin V., Faessler A., Simkovic F. & Vogel P., Uncertainties in the 0-Decay Nuclear Matrix Elements, *Czech. J. Phys.*, 56, 495-503, 2006.
[37] Vetterli M. C., Häusser O., Abegg R., Alford W. P., Celler A., Frekers D., Helmer R., Henderson R., Hicks K. H., Jackson K. P., Jeppesen R. G., Miller C. A., Raywood K. & Yen S., Gamow-Teller Strength Deduced from Charge Exchange Reactions on ^{54}Fe at 300 MeV, *Phys. Rev. C*, 40, 559-569, 1989.
[38] Rönnqvist T., Condé H., Olsson N., Ramström E., Zorro R., Blomgren J., Håkansson A., Ringbom A., Tibell G., Jonsson O., Nilsson L., Renberg P.-U., van der Werf S. Y., Unkelbach W. & Brady F. P., The ^{54,56}Fe(n,p)^{54,56}Mn Reactions at E_n = 97 MeV, *Nucl. Phys.*, A563, 225-246, 1993.
[39] Gove N. B. & Martin M. J., Log-f Tables for Beta decay, *At. Data Nucl. Data Tables*, 10, 205-317, 1971.
[40] Muto K., Bender E., Oda T. & Klapdor H. V., Proton-Neutron Quasiparticle RPA with Separable Gamow-Teller Forces, *Z. Phys. A*, 341, 407-415, 1992.
[41] Muto K., Bender E. & Klapdor H. V., Proton-Neutron Quasiparticle RPA

and Charge-Changing Transitions, *Z. Phys. A*, 333, 125-129, 1989.

[42] Anderson B. D., Lebo C., Baldwin A. R., Chittrakarn T., Madey R. & Watson J. W., Gamow-Teller Strength in the ^{54}Fe(p,n)^{54}Co Reaction at 135 MeV, *Phys. Rev. C*, 41, 1474-1485, 1990.

[43] Weaver T. A., Zimmerman G. B. & Woosley S. E., Presupernova Evolution of Massive Stars, *Astrophys. J.*, 225, 1021-1029, 1978.

[44] El-Kateb S., Jackson K. P., Alford W. P., Abegg R., Azuma R. E., Brown B. A., Celler A., Frekers D., Häusser O., Helmer R., Henderson R. S., Hicks K. H., Jeppesen R., King J. D., Raywood K., Shute G. G., Spicer B. M., Trudel A., Vetterli M. & Yen S., Spin-Isospin Strength Distributions for fp Shell Nuclei: Results for the ^{55}Mn(n,p), ^{56}Fe(n,p), and ^{58}Ni(n,p) Reactions at 198 MeV, *Phys. Rev. C*, 49, 3128-3136, 1994.

Fig. 1. (Color online) β^- decay rates of ^{54}Fe, as a function of stellar temperatures, for different selected densities. Densities are in units of gcm^{-3}. Temperatures are given in 10^9 K and $\log_{10}\lambda_{\beta^-}$ represents the log to base 10 of electron decay rates in units of sec^{-1}.

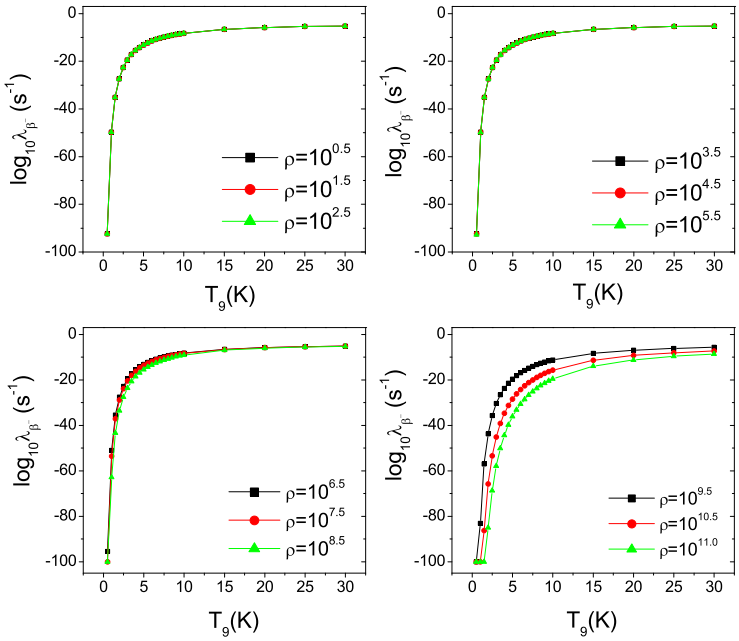

Fig. 2. (Color online) Same as figure 1 but for β^- decay rates of ^{55}Fe.

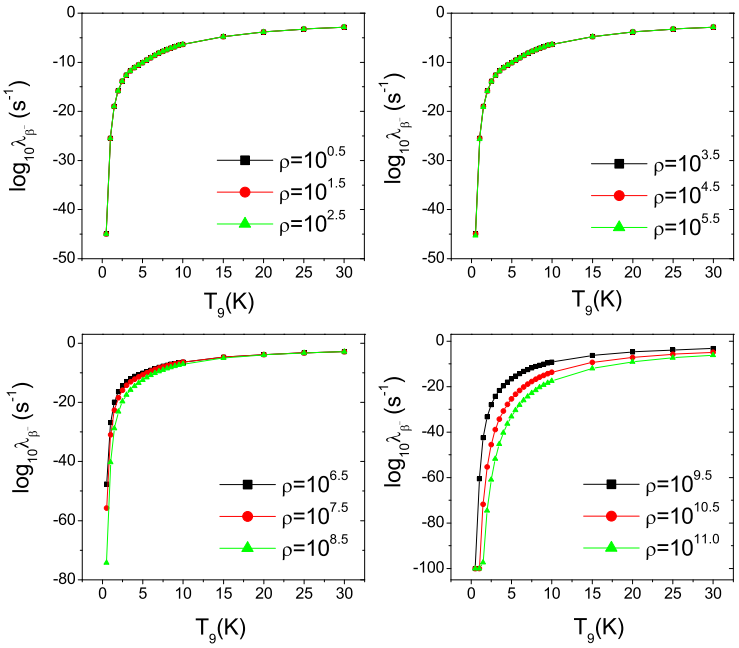

Fig. 3. (Color online) Same as figure 1 but for β^- decay rates of ^{56}Fe.

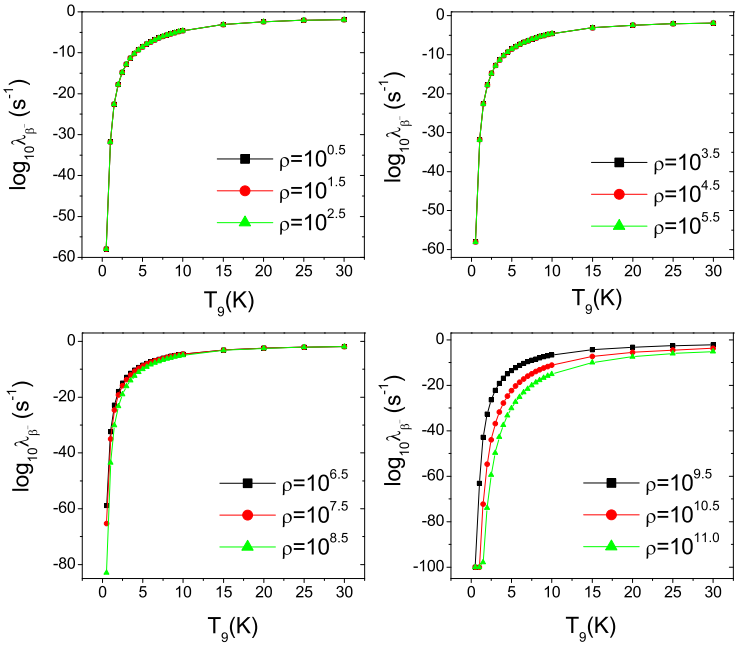

Fig. 4. (Color online) Same as figure 1 but for β^+ decay rates of ^{54}Fe.

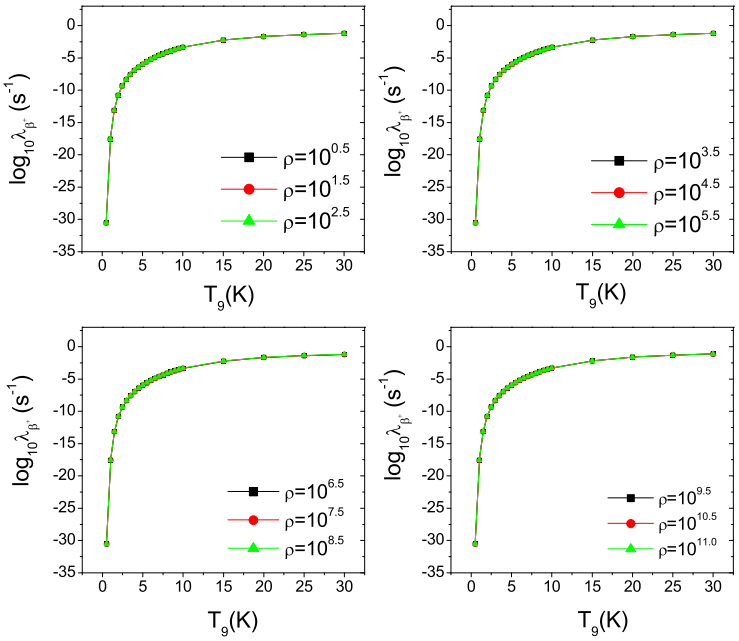

Fig. 5. (Color online) Same as figure 1 but for β^+ decay rates of ^{55}Fe.

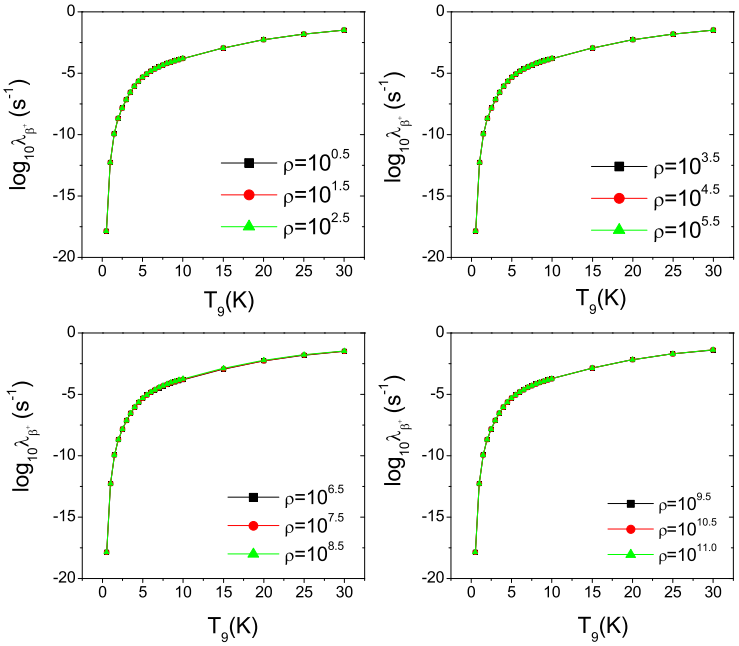

Fig. 6. (Color online) Same as figure 1 but for β^+ decay rates of ^{56}Fe.

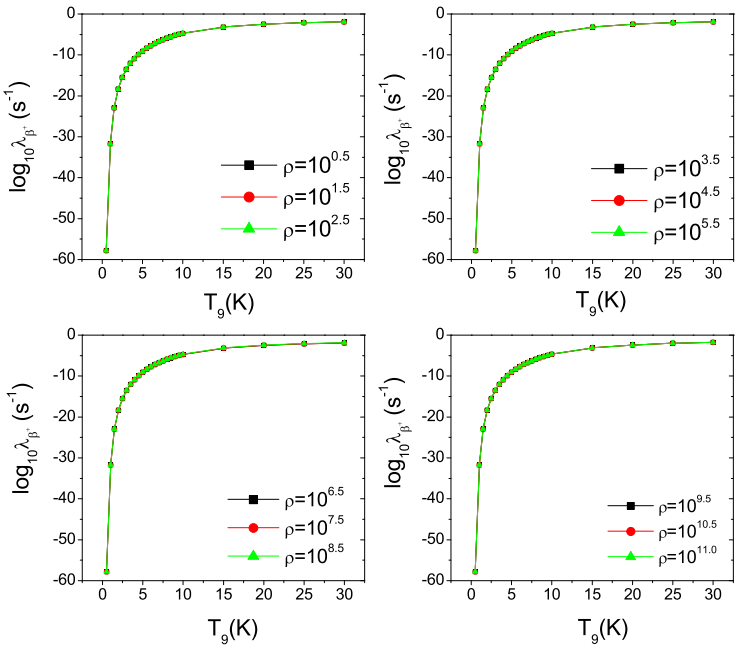

Fig. 7. (Color online) Ratios of reported β^+ decay rates to those calculated using LSSM (6) (upper panel) and FFN (4) (lower panel) for ^{54}Fe as function of stellar temperatures and densities. T_9 gives the stellar temperature in units of 10^9 K. In the legend, $log\rho Y_e$ gives the log to base 10 of stellar density in units of gcm^{-3}.

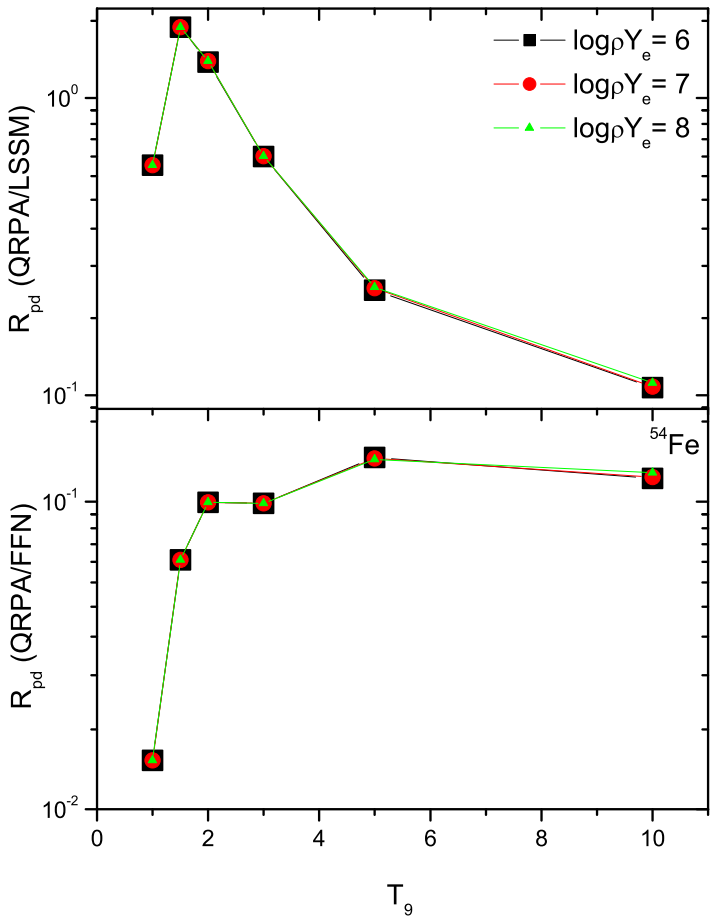

Fig. 8. (Color online) Same as figure 7 but for β^+ decay rates of ^{55}Fe.

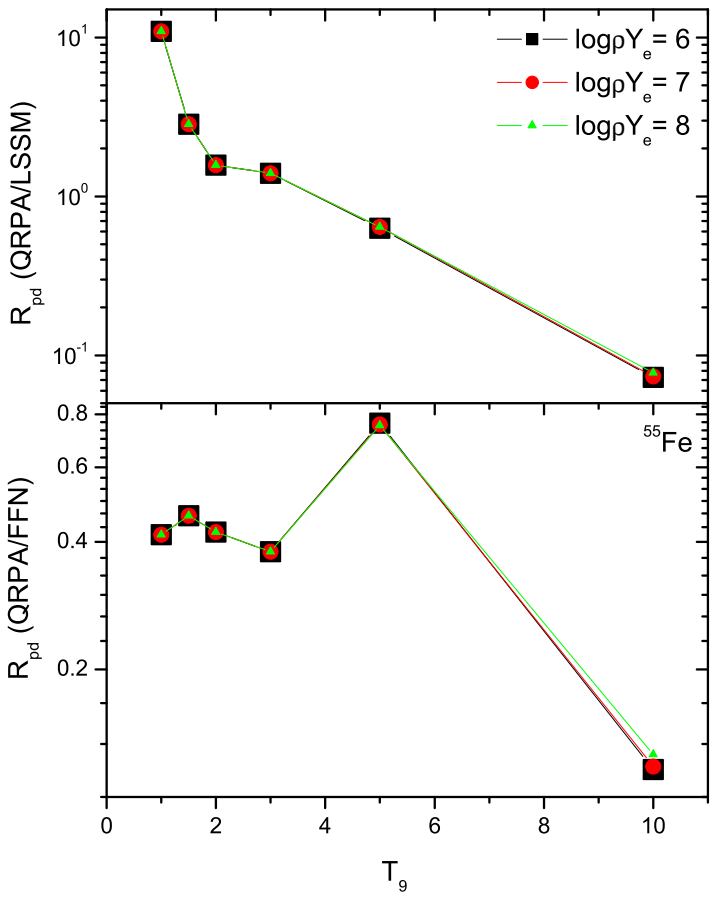

Fig. 9. (Color online) Same as figure 7 but for β^+ decay rates of ^{56}Fe.

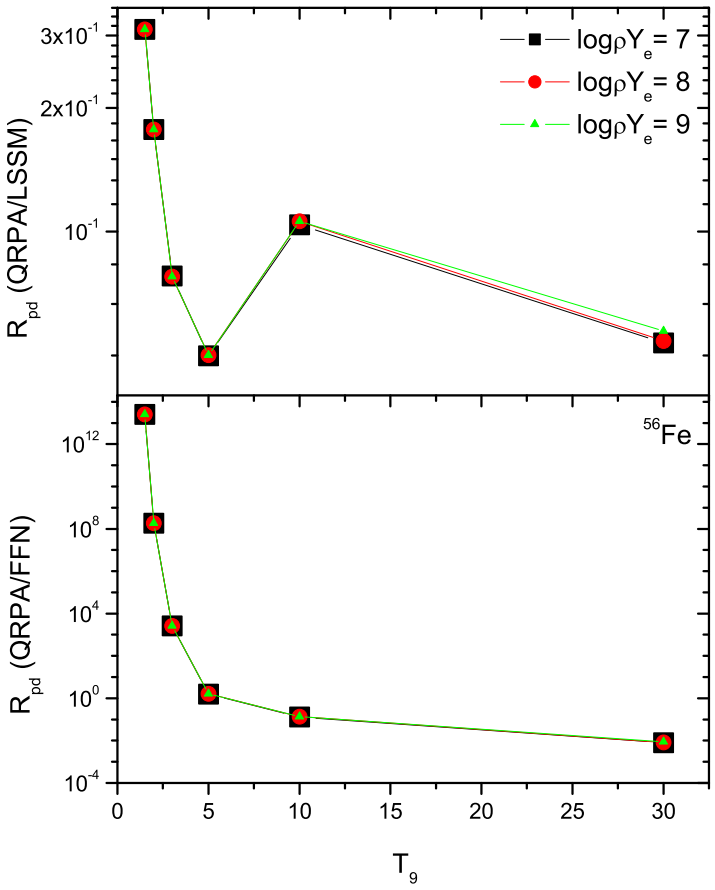

Fig. 10. (Color online) Same as figure 7 but for β^- decay rates of ^{54}Fe.

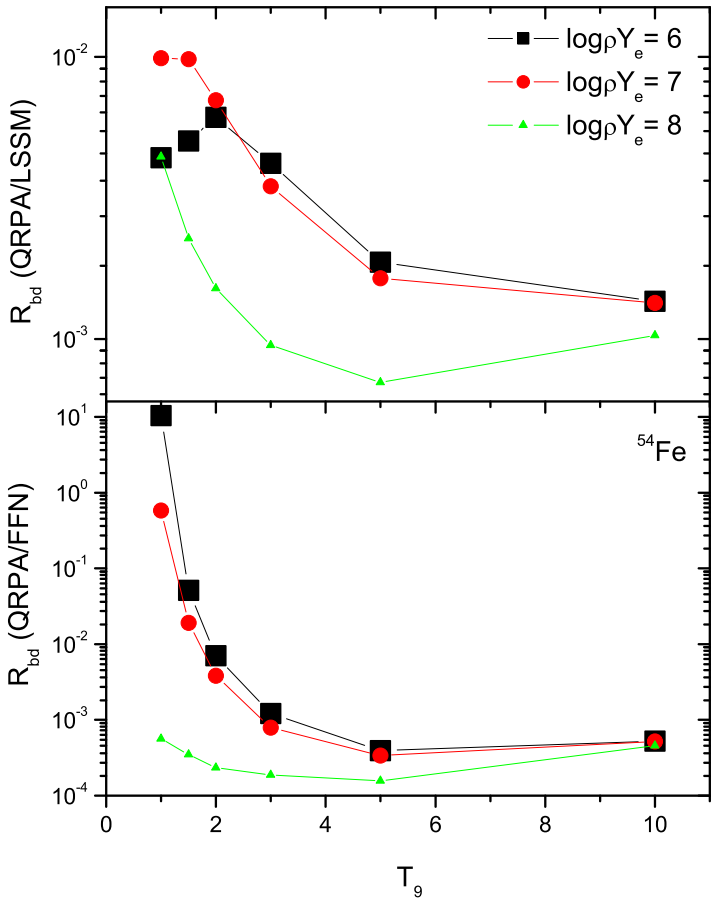

Fig. 11. (Color online) Same as figure 7 but for β^- decay rates of ^{55}Fe.

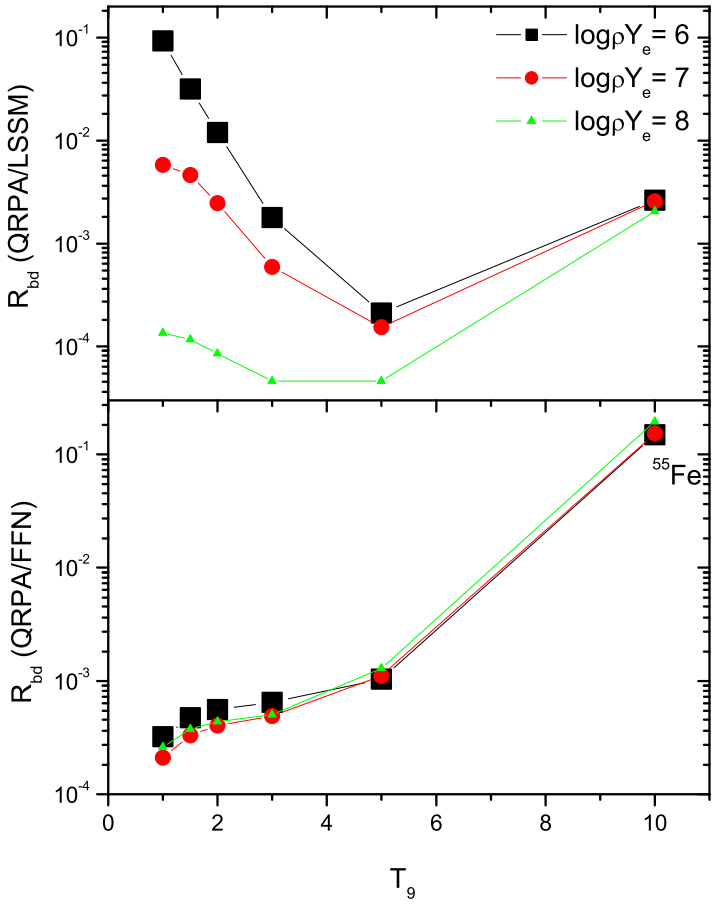

Fig. 12. (Color online) Same as figure 7 but for β^- decay rates of ^{56}Fe.

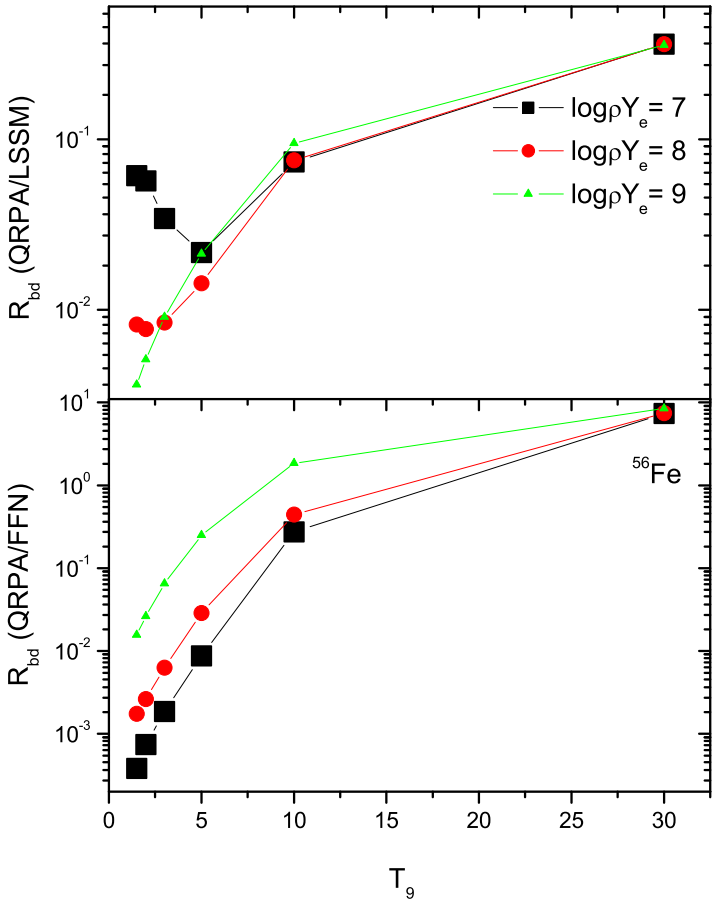

Fig. 13. Excited state Gamow-Teller (GT_-) strength distributions for ^{54}Fe. $E_i(E_j)$ represents parent (daughter) energy states.

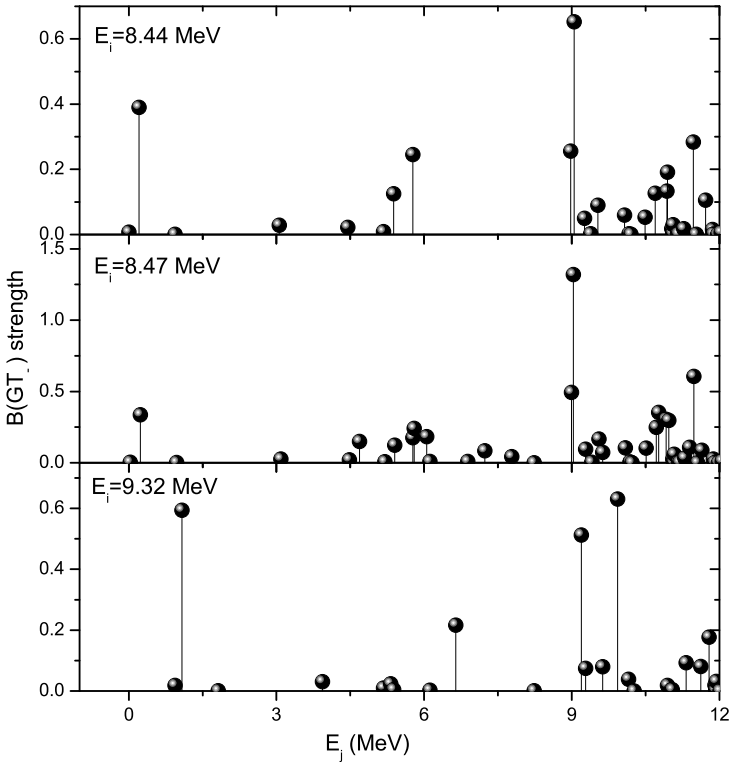

Fig. 14. Excited state Gamow-Teller (GT_-) strength distributions for ^{55}Fe. $E_i(E_j)$ represents parent (daughter) energy states.

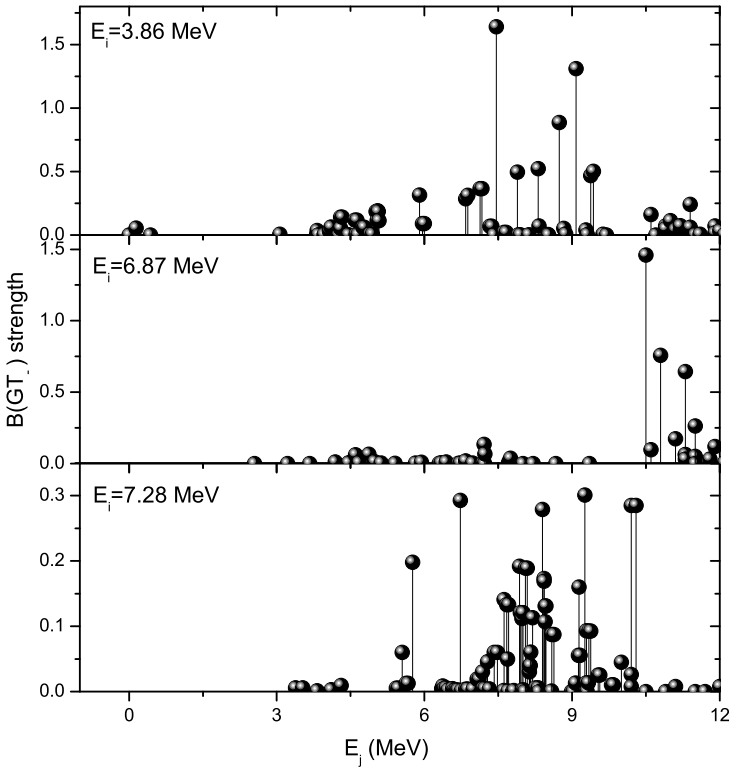

Fig. 15. Excited state Gamow-Teller (GT_-) strength distributions for ^{56}Fe. $E_i(E_j)$ represents parent (daughter) energy states.